ACS APPLIED MATERIALS & INTERFACES

Research Article

www.acsami.org

Tea Polyphenol–Functionalized Graphene/Chitosan as an Experimental Platform with Improved Mechanical Behavior and Bioactivity

Qian Huang,[†] Liying Hao,[†] Jing Xie, Tao Gong, Jinfeng Liao, and Yunfeng Lin*

State Key Laboratory of Oral Diseases, West China Hospital of Stomatology, Sichuan University, Chengdu 610041, People's Republic of China

Supporting Information

ABSTRACT: In this study, water-soluble, one-step highly reduced and functionalized graphene oxide was prepared via a facile, environment-friendly method by using tea polyphenol (TP), which acted as both reducing agent and stabilizer. The product obtained, that is, tea polyphenol–reduced graphene oxide (TPG), was used as a reinforcing building block for the modification of a mechanically weak chitosan (CS), TPG/CS. The morphology and physicochemical and mechanical properties of the composite were examined by various characterizations. The tensile strength and elastic modulus of CS were greatly improved by TPG, as compared to the findings for GO incorporation. Additionally, to our knowledge, this study is an in-depth analysis of the osteoblast functions of CS/TPG, including aspects such as cell cytotoxicity, proliferation, and expression of ossification genes, alkaline phosphatase (ALP), and Runt-related transcription factor (Runx2), which showed advantages in favorably modulating cellular activity. It was concluded that TPG/CS showed a higher elastic modulus, better hydrophilicity, and excellent biocompatibility than the pristine chitosan for promoting the proliferation and differentiation of osteoblasts, as well as for accelerating the expression of ALP and Runx2 (as shown by reverse transcription polymerase chain reaction (RT-PCR)). These results may provide new prospects for the use of TPG in the modification of biomaterials and for broadening the application of TPG in biological fields.

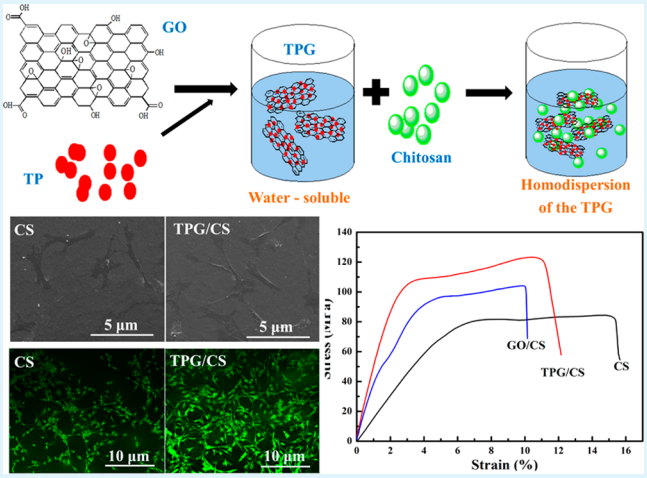

KEYWORDS: *graphene oxide, tea polyphenol, chitosan, osteoblast, mechanical properties*

1. INTRODUCTION

Recently, much attention has been paid to tissue engineering materials. In this field, chitosan (CS),[1] a nontoxic, antibacterial,[2] biodegradable, and biocompatible natural biopolymer, has attracted great interest in various applications, such as catalysts,[3] enzyme carriers, drug carriers,[4] biosensors,[5] medical implants,[6] filtration, and energy storage.[7] However, there are some obstacles that hinder its extensive use, such as low toughness, poor hydrolytic stability, and high degree of swelling, as well as high price as compared to that of conventional plastics. To overcome these mechanical and scientific challenges, CS-based composites have been studied to expand the range of applications of CS.[8,9] Blending of synthetic carbonaceous materials with CS, for example, in GO/CS and CNT/CS, has been reported in recent years and has been found to promote cytocompatibility and physicochemical properties of CS.[10,11]

Graphene, a novel carbon-based material, has been extensively studied due to its excellent mechanical, thermal, physical, electronic, chemical, and biological properties.[12−15] Moreover, graphene oxide contains numerous reactive oxygen functional groups, such as abundant epoxide, hydroxyl, and carboxylic groups, which can provide a large number of reactive sites for chemical functionalization.[16−18] Therefore, it can be used as a building block to synthesize versatile functional materials for a variety of applications. Until date, this new carbon-based material has been widely applied in biosensor development, imaging, drug delivery, bacterial inhibition, and photothermal therapy. Furthermore, graphene is being analyzed as a reinforcement material for enhancing the modulus and mechanical strength of polymers.[19,20] During the past few years, diverse methods have been proposed to prepare graphene, such as mechanical or ultrasonic exfoliation,[21] epitaxial growth, chemical vapor deposition,[22] and chemical reduction of GO.[23] Chemical reduction, which is the most commonly used method, uses highly toxic reducing agents, which could be

Received: July 13, 2015
Accepted: September 3, 2015
Published: September 3, 2015

DOI: 10.1021/acsami.5b06300
ACS Appl. Mater. Interfaces 2015, 7, 20893−20901

detrimental to biorelated applications.[24] Moreover, reduced graphene oxide (rGO) easily tends to form aggregates due to van der Waals interactions between graphene planes.[23] Therefore, functionalization of graphene is still highly desirable.

Tea polyphenols (TPs), which are biocompatible and biodegradable, act as both reducing agents and stabilizers that reduce and modify GO so as to provide tea polyphenol−reduced graphene oxide (TPG).[25,26] TP has many applications in medical treatment, such as anticancer effects,[27] promotion of cardiovascular health,[28] and improvement of immunity.[29] Furthermore, it also provides a promising approach for mitigating bone loss, which is of great assistance in reducing the risk of osteoporosis in the elderly population.[30,31] There are many reactive oxygen sites on the surface of TPG, which can be easily incorporated within CS and efficiently prevent rGO from agglomerating. Wang et al. have previously reported this method and prepared TPG/CS. However, they just studied the TPG/CS from the morphology and tested its physical properties. TPG is then applied in NIR-mediated photodestruction of cancer cells afterward.[32] More detailed materials detection and its biological properties are still unknown and need further study.

In the present study, the complementary properties of CS and TPG, that is, biocompatibility and nontoxicity, were utilized to obtain a biocompatible and mechanically strong biocomposite by dispersing TPG sheets in CS solution. The morphology and the structural and mechanical properties, as well as the bioactivity, of TPG/CS have been evaluated in this study. The TPG/CS composite showed strong mechanical property and low cytotoxicity, as well as promoted the expression of ALP and Runx2, which provided a guiding significance for the modification of the biomaterials. It is believed that, with these complementary advantages, TPG/CS could have great potential for use in the tissue engineering field.

2. MATERIALS AND METHODS

2.1. Materials. The materials used in this study were as follows: low molecular weight CS (BR 99%, as provided by the supplier), which was obtained from Xiya Reagent; the tea polyphenols used in our experiment were purchased from Fuzhou Corona Science and Technology Co., Ltd., which are separated from green tea. Epigallocatechin gallate (EGCG) is the main bioactive compound, which accounts for >50% of the total tea polyphenols (Figure S1), along with acridine orange (AO), acetic acid, sodium hydrate (NaOH), phosphate-buffered saline (PBS) solutions (pH 7.40), and deionized water. Furthermore, Dulbecco's modified Eagle's medium (DMEM), fetal bovine serum (FBS), and 0.25% trypsin-EDTA were obtained from Gibco Life Technologies. Collagenase I was from Biosharp, and Cell Counting Kit-8 (CCK-8) was from Dojindo Laboratory. All chemicals were of analytical grade and were used as received without further purification.

2.2. Fabrication of the TPG/CS. The GO was obtained using the modified Hummer's method. A suspension of 2 mg/mL GO was obtained for further experiments. TPG was synthesized by following the steps reported in a previous study. Briefly, 600 mg of TP was dissolved in 150 mL of double distilled water; then, 50 mL of 2 mg/mL GO solution was added. The liquid mixture was then placed in Teflon-lined stainless-steel autoclave (50 mL) and kept at 100 °C for 8 h; the TPG obtained was then kept in the bag filter and was soaked in double distilled water for the purification of the product.

CS solution (1%) was prepared by dissolving 1 g of CS in 100 mL of 4% acetic acid aqueous solution. The solution was stirred until it became transparent; it then was allowed to stand for 24 h and the insoluble material was removed. TPG was added, followed by ultrasound treatment for 1 h. The solution was then stirred for 3 h. After being stirred, the TPG/CS solution was poured in a flat dish, which was then placed in a baking oven at 37 °C until it dried completely. The film obtained then was placed in 0.2 mol/L disodium hydrogen phosphate solution for 30 min to neutralize the acetic acid. Next, the materials were washed using double distilled water. The GO/CS film was prepared using the same steps, with TPG being replaced by GO.

2.3. Characterization of the Samples. Analysis of the surface and fracture-surface morphology of the materials was carried out with a field emission scanning electron microscope (FE-SEM, Inspect F) that had a digital camera (MEGA VIEW-II DOCU) and was operated at 20.00 kV. Atomic force microscope (AFM) measurements were performed in tapping mode with Shimadzu SPM-9700. X-ray diffraction (XRD) measurements were performed using an X'Pert Pro X-ray diffractometer (Philips) with Cu Kα radiation (λ = 1.5406 Å). Step scanning was carried out at 2θ intervals from 5° to 90°. Fourier transform infrared (FTIR) spectroscopy was performed on a Thermo Nicolet IS10 FT-IR spectrometer with KBr pellets in the range of 500−4000 cm^{-1}. Raman spectroscopy was carried out using a LabRam HR Raman system; the excitation source is a 532 nm laser. The tensile properties and elongation at break of the materials were measured using the INSTRON model 5565 test machine at room temperature; the strain rate was 1 mm/min. The values were the average of 10 measurements. Hydrophilic properties were tested on DataPhysics' OCAH 200 optical high-speed contact angle measuring system.

2.4. Cell Proliferation and Adhesion. *2.4.1. Primary Cell Culture.* Twenty-four h-old SD rats (purchased from Sichuan University Animal Center) were sacrificed by fast decapitation in accordance with the International Guiding Principles for Animal Research (1985). Rat calvariae were dissected and washed extensively in sterile PBS to remove tissue debris. They then were cut into 1 × 1 mm fragments and incubated in 0.25% trypsase for 20 min at 37 °C. Finally, the supernatants were discarded, and the calvariae were subsequently rinsed in PBS and subjected to digestion in DMEM containing 0.075% type I collagenase for 60 min at 37 °C. After neutralization of the collagenase, the osteoblasts (OBs) released during the subsequent digestions were spun down, collected, and combined after centrifugation for 10 min at 1000 rpm. The cells were then seeded in DMEM supplemented with 10% FBS, 1% penicillin, and streptomycin, and then cultured at 37 °C in 5% CO_2/95% air until 80% confluence was achieved.

2.4.2. CCK-8 Assay and Imaging Analysis. OB cells at 1 × 10^4/mL density were seeded into a 96-well plate with 200 μL of media in each well. Proliferation of the cells cultured on the sterilized pellets (6.5 mm in diameter) in the 96-well plate was analyzed using the Cell Counting Kit-8 (CCK-8) assay at different time points (24, 48, and 72 h after seeding). The procedures used were as follows: Cells were washed with PBS after removing cell culture medium, and 200 μL of culture medium (no serum), enriched with 10% CCK-8 reagent, was added to each specimen in the 96-well plates, and the plates were incubated for 2 h at 37 °C. Finally, the optical density of the solution in each well was measured at a wavelength of 450 nm using a microplate reader (VariOskanFlas 3001; Thermo, U.S.). To better evaluate cell proliferation except for the CCK-8, we also performed AO staining for cells with the materials cultured for 1, 3, and 5 d. The OBs were washed with PBS solution and stained with 100 μg/mL AO for 5 min. After the samples were washed twice with PBS, they were observed under an inverted microscope (Olympus IX 710, Tokyo, Japan).

2.4.3. Cell Adhesion and Morphology Analyses. Cell adhesion and morphology were investigated using an SEM. For SEM analysis, after 24 h incubation, the cell culture medium was removed, and the samples were fixed with 2.5% glutaraldehyde overnight and then dehydrated in a graded ethanol series (50%, 60%, 70%, 80%, 90%, and 100%) for 10 min at each level. The specimens were then dried in an exhaust hood at room temperature. The processed specimens were then mounted on specimen holders, coated with a thin layer of gold, and examined using SEM.

2.4.4. Reverse Transcription Polymerase Chain Reaction (RT-PCR). After the osteoblasts were seeded on CS and TPG/CS for the culture times of 1, 2, 4, and 7 days, total RNA was extracted and

DOI: 10.1021/acsami.5b06300
ACS Appl. Mater. Interfaces 2015, 7, 20893−20901

Table 1. Primer Sequences Applied for RT-PCR

primer	fragment length (bp)	upstream sequence	downstream sequence
GAPDH	233	ACAGCAACAGGGTGGTGGAC	TTTGAGGGTGCAGCGAACTT
Runx2	106	CCTCTGACTTCTGCCTCTGG	GATGAAATGCCTGGGAACTG
ALP	101	CCTGACTGACCCTTCCCTCT	CAATCCTGCCTCCTTCCACT
BMP-2	102	TCAAGCCAAACACAAACAGC	CCACGATCCAGTCATTCCA
BMP-4	101	GACTTCGAGGCGACACTTCT	AGCCGGTAAAGATCCCTCAT

purified using a total RNA Kit (Bioteke, Beijing). The total RNA concentration and purity were determined using a microplate reader (VariOskanFlas 3001; Thermo, U.S.), and the reverse transcription was carried out with the PrimeScript RT Reagent Kit with gDNA Eraser (TaKaRa). RT-PCR was carried out using a reaction mixture containing 12.5 μL 2× Taq PCR MasterMix (TIANGEN), 2 μL of specific primer pairs (Table 1), and 9.5 μL of RNase-free water (TIANGEN). The PCR amplification procedure used in this study was as follows: predenaturation at 95 °C for 3 min; 30−35 cycles of denaturation at 95 °C for 30 s, annealing at 63 °C for 30 s, and synthesis at 72 °C for 30 s; and final extension at 72 °C for 10 min. PCR products were analyzed by agarose gel electrophoresis. The same cDNA sample was used for detecting the expression of different genes. The PCR products were analyzed using the Gel Doc 2000 system (BIO RAD, U.S.) and the Quantity One software. The expression of the markers was normalized to the expression of GAPDH by imaging analysis performed using the BioImaging System GeneGenius with the acquisition software Image Pro Plus 6.0.

3. RESULTS AND DISCUSSION

3.1. Mechanical Properties of CS, GO/CS, and TPG/CS. To understand the reinforcing effect of GO and TPG on the surface of CS, different concentration gradients of TPG and GO of chitosan (0, 0.1, 0.2, 0.5, 1 wt %) were tested (Figure S2). As shown in Figure S2, the stress of the composites was improved with the increase of the content of GO and TPG, up to 0.5 wt %. However, the tenacity of the composites decreased at high content. Obviously, the stress and tenacity of the composites were not dominant at higher content (1 wt %). Taking the stress and tenacity of the composites into account, 0.5 wt % TPG and GO showed the best mechanical properties, which would be used in our following experiments. Additionally, the stress−strain curves and the comparison of the elastic modulus and elongation at break of 0.5 wt % TPG/CS, 0.5 wt % GO/CS, and CS films are shown in Figure 1A,B, respectively. The CS film exhibited the poorest mechanical properties. The introduction of GO improved the mechanical properties of CS, but the stress−strain curve was not steady and had the lowest breaking elongation rate, which indicated defects in the composites and suggested uneven dispersion of GO in the CS because of aggregation. TPG/CS exhibited the best mechanical properties on analysis of elastic modulus, which was attributed to the homogeneous dispersion of the TPG in the CS polymer and the strong bonding between CS and the phenolic hydroxyl group of TP (Figure 1B). Also, the elastic modulus of TPG/CS (4.23 ± 0.21 GPa) was higher than that of GO-chitosan (3.5 ± 0.2 GPa).[9] Additionally, there are many reactive sites (phenolic hydroxyl group), and it is nontoxic for TP as reducing agent and modifier. Therefore, we chose TPG for the modification of CS instead of GO, and the bioactivities of TPG/CS were investigated in the ensuing experiments.

3.2. Morphological Analysis and Surface Properties of the Materials. SEM and AFM were used to analyze the surface properties of the materials. The TPG obtained was examined by AFM (Figure 2A); before the examination, the TPG solution was sonicated for 30 min. As depicted in Figure 2B, the average thickness of TPG was about 1.58 nm, which was greater than that of the prepared single-layer graphene (0.93 nm); this difference was attributable to the attachment of TPs on both sides of the graphene sheet. The morphologies of CS have been presented in Figure 3A and C; the pure CS comprised monodispersed nanoparticles (diameter, about 50 nm). As for TPG/CS (Figure 3B, SEM), the CS nanoparticles were seeded on the surface of TPG; that is, a "sandwich" structure was formed through hydrogen-bond interactions, electrostatic attractions, or amide linkages between the amino and hydroxyl groups of CS, and the hydroxyl groups and residual carboxyl groups of TPG (Scheme S1). The above-mentioned interactions between CS and TPG may play an important role in improving the mechanical properties of the composite (TPG/CS). Also, the results demonstrated that most of the TPG sheets were fully exfoliated and well dispersed in the CS matrix, as well as parallel to the composite. The above-mentioned interactions between CS and TPG may play an important role in improving the mechanical properties of the composite (TPG/CS). The topographic height of TPG/CS increased to about 3−4 nm (not shown in the picture), indicating that the CS nanoparticles were successfully grafted onto the surface of TPG (Figure 3D, AFM). In contrast, the composite appeared relatively coarse because a minor portion of TPG would still remain as stacked layers, although the TPG

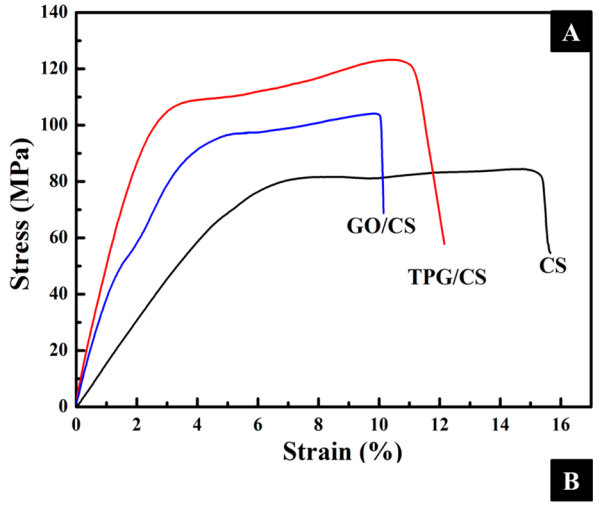

	Elastic Modulus (GPa)	Elongation at break (%)
CS	1.22±0.12	14.61±0.66
GO/CS	3.12±0.19	10.22±0.62
TPG/CS	4.23±0.21	11.95±0.58

Figure 1. Mechanical properties of CS, GO/CS, and TPG/CS. (A) Stress−strain curves of CS, GO/CS, and TPG/CS. (B) Elastic modulus and elongation at break of CS, GO/CS, and TPG/CS.

DOI: 10.1021/acsami.5b06300
ACS Appl. Mater. Interfaces 2015, 7, 20893−20901

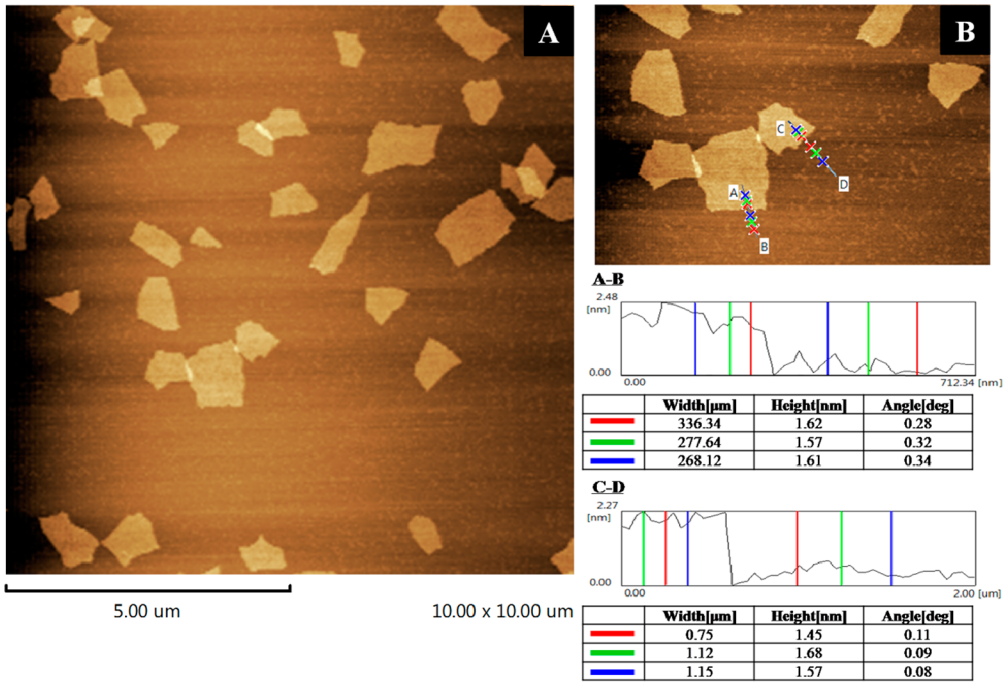

Figure 2. (A) Tapping mode AFM image of TPG sheet. (B) The measurement of lateral width and thickness.

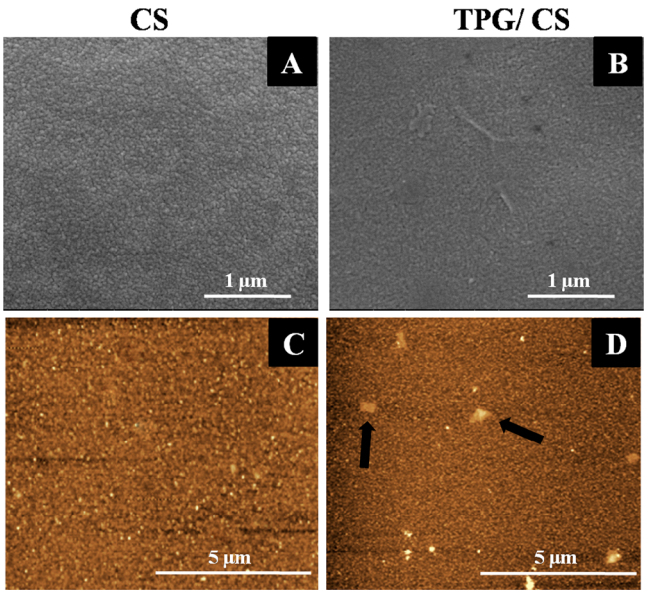

Figure 3. Surface morphology of the CS and TPG/CS. SEM (A) and AFM (C) images of CS; SEM (B) and AFM (D) images of TPG/CS. The black arrows point at the TPG sheets.

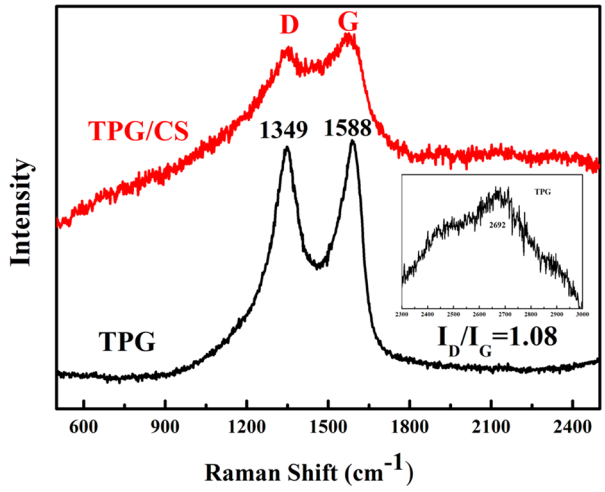

Figure 4. Raman spectra of TPG and TPG/CS. Inset: Raman spectrum of TPG at about 2700 cm^{-1}.

was primarily exfoliated to monolayer platelets (Figure 2B). Meanwhile, the Raman spectrum of these materials (TPG, CS, TPG/CS) was also applied to confirm the carbon structure of TPG and discuss about single- and/or multilayer properties of TPG sheet in the composites. As shown in Figure 4, TPG has the typical G band at 1588 cm^{-1}, D band at 1349 cm^{-1}, and 2D band at 2692 cm^{-1}, which is in accordance with the values of single-layer graphene from the related references.[33,34] The G band comes from the E_{2g} phonon of C sp^2 atoms, and the D band is ascribed to edges, other defects, and disordered carbon atoms. The intensity ratio (I_D/I_G) of the D band to G band of TPG is increased to 1.08 as compared to that of GO (0.92, Figure S3), which suggested the incomplete recovery of the graphene structure. Although the 2D band was used to verify the number of graphene layers, the Raman spectrum of CS was restricted because of its fluorescence (Figure S3). The 2D band of TPG/CS was covered, and the G band of the composites was used to discuss the single- and/or multilayer properties of the TPG sheet in the composites. As shown in Figure 4, the G band at 1583 cm^{-1} was observed, which suggested single-layer TPG existed in the composites. The results were in agreement with those of AFM.

Moreover, the fracture surfaces of the composite and pure CS films were observed as shown in Figure 5A–D. As compared to pure CS (Figure 5A and D), TPG was well dispersed across the composite surface (Figure 5B and D), and CS nanoparticles were seeded on both sides of TPG. The composite approach may improve the mechanical properties of CS.

DOI: 10.1021/acsami.5b06300
ACS Appl. Mater. Interfaces 2015, 7, 20893−20901

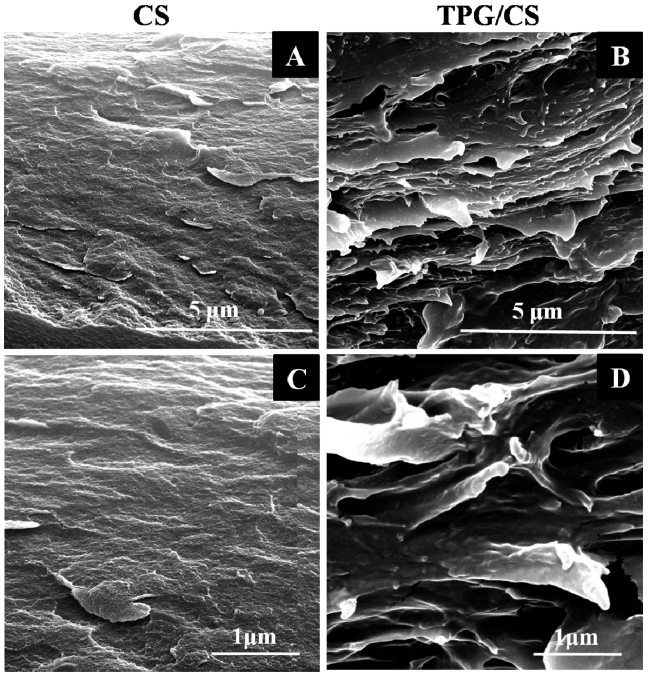

Figure 5. SEM images of CS (A,C) and TPG/CS (B,D) fracture surfaces.

3.3. XRD, FTIR, and Contact Angle Analyses. XRD was used to evaluate the effect of the TPG on the crystallinity of the CS in the biocomposite, which is shown in Figure 6A. The TPG showed a broad peak at 25.6°, which was quite close to that of graphene layers in pristine natural graphite, and the characteristic absorption peak (2θ = 10°) of the GO disappeared, indicating that the functional groups of GO were successfully removed.[35] For the pristine CS, the characteristic peaks seen at 2θ values of 8.24° and 11.33° corresponded to the hydrated crystalline structure, and that seen at 23.8° corresponded to the amorphous structure.[36,37] The TPG/CS showed the main peaks of CS, which indicated that the incorporation of TPG did not alter the crystalline structure of CS. A new sharp peak was observed at 9.23°, which may be because of interaction of TPs with CS. To identify the functionalized chemical groups in the three materials, FTIR was used to study their chemical constitution. As shown in Figure 6B, the dominant peaks of CS existed at 3439, 1653, and 1592 cm^{-1}, which correspond to O−H and N−H hydrogen band stretches, and C−O stretching of the acetyl group, and N−H bending and stretching, respectively.[38,39] The band at 1070 cm^{-1} was associated with the skeletal vibration of the bridge C−O stretch of glucosamine residue. In the spectrum of TPG, we observed dominant peaks at 1032, 1236, and 1653 cm^{-1}, which were ascribed to the stretching and in-plane deformation of O−H in TP,[40] and C═C bonds of the graphene associated with skeletal vibrations of unoxidized graphite domains, respectively. As compared to GO (Figure S4), the oxygen functional groups decreased, which suggested GO was successfully reduced with TP. For TPG/CS, the spectra contained the dominant peaks of CS and TPG, which suggested there were some interactions between CS and TPG. These interactions may have a strong impact on the mechanical properties. The dominant peaks at 1032, 1236, and 1653 cm^{-1} of TPG were decreased, which was due to the low content of TPG.

The results of hydrophobicity measurement showed that, in the case of introduction of TPG, the hydrophilic angle of the composite was a little smaller than that of pure CS, implying

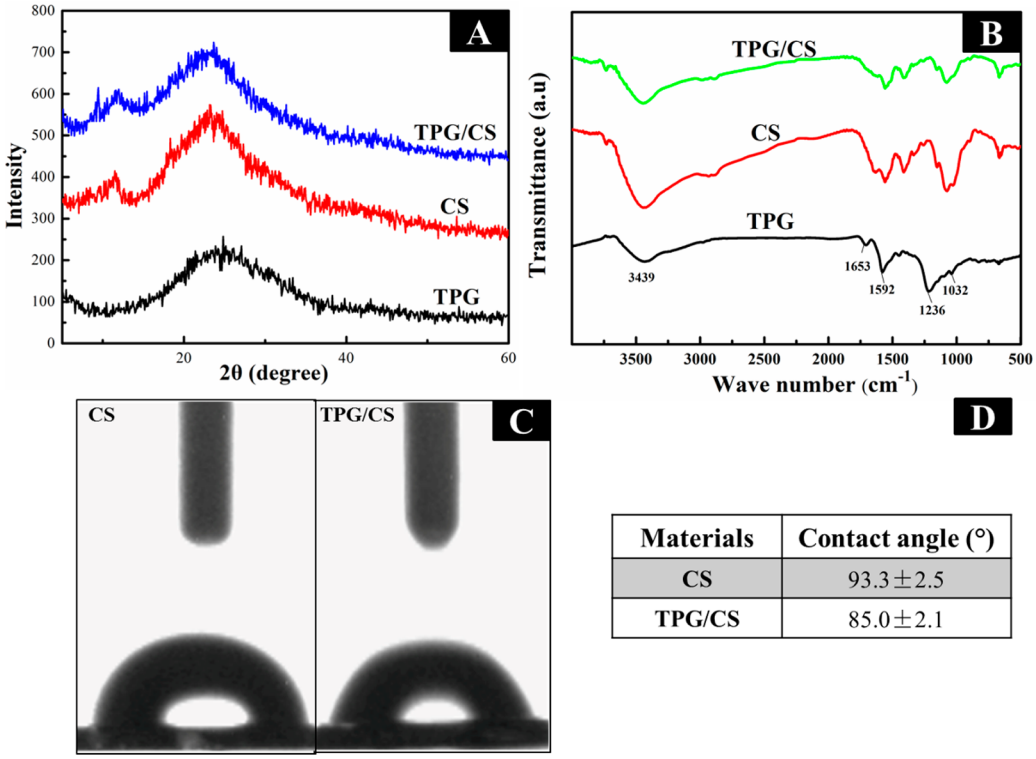

Materials	Contact angle (°)
CS	93.3±2.5
TPG/CS	85.0±2.1

Figure 6. (A) XRD spectra and (B) FTIR spectra of CS, TPG, and TPG/CS. (C) Contact angle test of CS and TPG/CS. (D) Contact angle value of CS and TPG/CS.

DOI: 10.1021/acsami.5b06300
ACS Appl. Mater. Interfaces 2015, 7, 20893−20901

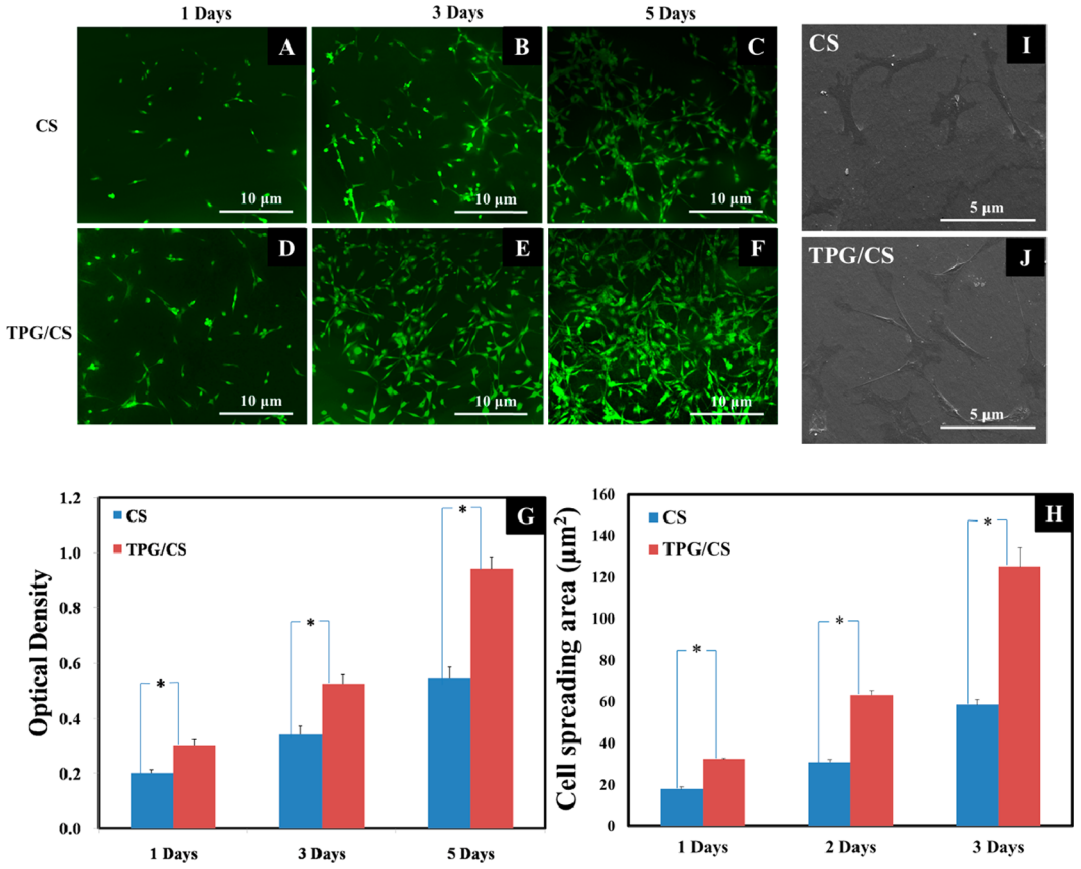

Figure 7. (A–F) AO staining of the osteoblasts seeded on the materials on 1, 3, and 5 days. (I,J) SEM electron micrographs of the fixed osteoblasts seeded on samples CS and TPG/CS. (G) CCK-8 assay of osteoblasts seeded on samples CS and TPG/CS on 1, 3, and 5 d for cell viability and proliferation. Statistical analysis shows significant difference in the three time points (*$p < 0.05$, $n = 3$). (H) Analysis of cellular area on samples CS and TPG/CS on 1, 3, and 5 days. Statistical analysis shows significant difference in 1, 3, and 5 days (*$p < 0.05$, $n = 3$).

better hydrophilicity (Figure 6C,D), which may be due to the hydrophilic group of the TPG and the adsorbed TPs. In previous reports, it was shown that the hydrophilicity of a material's surface may promote bone formation; a possible reason is that the hydrophilic surface has preferential solubility with respect to divalent ions.[41] Moreover, the increased hydroxyl content on the hydrophilized surface may also contribute to promoting osteogenic differentiation of the TPG-modified CS.[42]

3.4. In Vitro Cellular Assay. *3.4.1. CCK-8 Assay and Imaging Analyses.* As is shown in Figure 7G, TPG/CS exhibited higher OD values than CS after 1 d of culturing. This trend was more evident over time, indicating that the dissimilarities in cell viability gradually increased with increase in time. The difference had statistical significance (*$p < 0.05$, $n = 3$). The CCK-8 assay results suggested that modified CS (TPG/CS) promoted cell proliferation, implying a beneficial effect of TPG on cell growth.

To further determine the viability of the osteoblast cells, the cells were planted on the three materials and incubated for 1, 3, and 5 d. They were then stained with AO, and cell images were obtained (Figure 7A–F). The fluorescent images revealed differences in cell numbers on CS and TPG/CS 1 day after culture. After 3 d of culturing, the osteoblasts grew evidently faster on the TPG/CS. This difference was amplified after 5 d of incubation. The cellular area was also calculated using ImageJ (Figure 7H). Accordingly, cell spreading area on the TPG/CS was higher than the CS group at each time point. Besides, statistical difference was found between the different groups (*$p < 0.05$, $n = 3$). In conclusion, cell morphology was also affected by CS composites with different mechanical properties.

In the electron microscope image of the fixed cells (Figure 7I,J), more cells were found to be attached on the TPG/CS and the cell morphology was affected by the film type, while cells were distributed unevenly and did not spread well on the pure CS films. The cells on the TPG/CS were distributed more evenly and spread well. The elongated morphology observed on TPG/CS may indicate promotion of signal conduction between osteoblasts.

3.4.2. RT-PCR. To study the variation in gene expression on different materials, RT-PCR was performed after 1, 2, 4, and 7 days of cultivation. The markers assigned to rat osteoblasts were ALP, Runx2, BMP-2, and BMP-4.[43−45] Expression of GAPDH is the verification of similar amounts of RNA in these samples (Figure 8). Quantitative analysis of mRNA values normalized to those of the housekeeping gene GAPDH (Table 2) demonstrated that the expression of ALP and Runx2 increased reposefully over time and that the levels for the TPG/CS group were higher than those of the CS group. BMP-2 and BMP-4 did not show obvious variation over time, perhaps because in the cell experiment, the bone structure was irregular. The results showed significant differences in terms of ALP and Runx2 gene expression on the two materials.

Various bone formation-related genes play a part in osteogenesis. ALP activity can reflect the degree of differentiation of osteoblasts.[46] Runx2 mediates regulation of the

DOI: 10.1021/acsami.5b06300
ACS Appl. Mater. Interfaces 2015, 7, 20893−20901

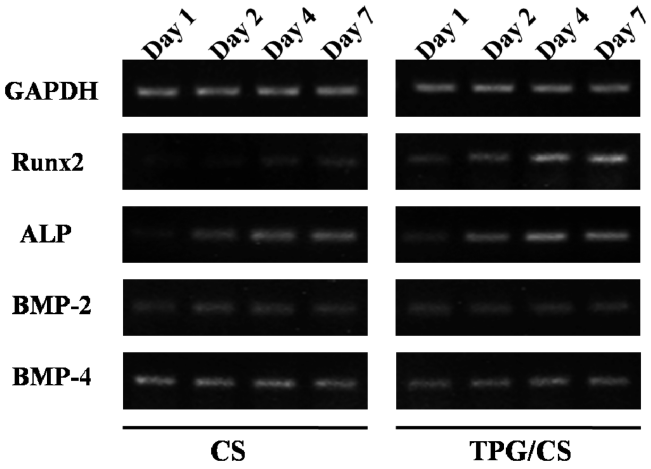

Figure 8. Gene expression of the osteoblast-related markers ALP, Runx2, BMP-2, and BMP-2, as well as the housekeeping gene GAPDH, after 1, 2, 4, and 7 days of cultivation.

transcription and differentiation of osteoblasts and regulates the development of osteoblasts.[47] Upregulation of ALP and Runx2 suggested that the TPG-modified CS provided a better cellular differentiation stimulus for the osteoblasts. Thus, this work will provide a new and good building block for the modification of tissue engineering materials.

The stiffness of the matrix also played a role in cell differentiation and morphology. In previous reports, it was proved that variation in elastic modulus can effectively influence the adhesion, cytoskeleton, and the differentiation of preosteoblast, because it had important significance in bone formation, remodeling, and repair of bone tissue.[48,49] As it was also observed in our experiment, on the stiffer substrates osteoblast, related genes were up-regulated and cells had better spreading morphology. Therefore, we suggest that the reinforcement effect by TPG on the CS influenced the morphology and differentiation of osteoblasts to some degree.

4. CONCLUSIONS

In summary, a TPG-incorporated CS (TPG/CS) composite was prepared and used to enhance the mechanical properties of CS and favorably modulate cellular activity. Our results demonstrated that the TPG/CS composite showed better mechanical properties than GO/CS. Furthermore, good dispersivity of TPG in the CS was observed by SEM and AFM. The TPG/CS composite promoted the proliferation and differentiation of osteoblasts to a greater extent, which is an important aspect for the application of the biomaterials in bone tissue engineering, especially in the case of diseases such as osteoporosis. Furthermore, the composite promoted the expression of ALPase and Runx2, which could reflect in and regulate the differentiation of osteoblasts. As compared to the results of previous studies that used GO to prepare the composite, our TPG/CS composite showed similar or better improvements in mechanical properties and improved bioactivity; furthermore, it had low cost of production, good dispersivity, and low toxicity. Taking the versatility of TPG into account, the TPG/CS biocomposite might have potential uses in a broader range of biorelated applications, such as tissue engineering and bioimaging. However, further studies should be performed to test the related biocomposite in clinical trials.

■ ASSOCIATED CONTENT

Supporting Information

The Supporting Information is available free of charge on the ACS Publications website at DOI: 10.1021/acsami.5b06300.

Additional data including chemical structure, stress−strain curves, Raman spectra of CS and GO, and FTIR spectra of GO, TP, and TPG (PDF)

■ AUTHOR INFORMATION

Corresponding Author

*Tel.: 028-85582167. Fax: 86-28-85503487. E-mail: yunfenglin@scu.edu.cn.

Author Contributions

†Q.H. and L.H. contributed equally to this work.

Notes

The authors declare no competing financial interest.

■ ACKNOWLEDGMENTS

This work was funded by the National Natural Science Foundation of China (81470721, 31170929) and the Sichuan Province Science and Technology Support Program (2014SZ0019-3).

■ REFERENCES

(1) Yalpani, M.; Hall, L. D.; Tung, M. A. Unusual Rheology of a Branched, Water-Soluble Chitosan Derivative. *Nature* **1983**, *302*, 812−814.

(2) Wu, Y. B.; Yu, S. H.; Mi, F. L. Preparation and Characterization On Mechanical and Antibacterial Properties of Chitsoan/Cellulose Blends. *Carbohydr. Polym.* **2004**, *57*, 435−440.

(3) Xue, Z.; Sun, X.; Li, Z. CO_2 as a Regulator for the Controllable Preparation of Highly Dispersed Chitosan-Supported Pd Catalysts in Ionic Liquids. *Chem. Commun.* **2015**, *51*, 10811−10814.

(4) Lin, Q.; Bao, C.; Yang, Y. Highly Discriminating Photorelease of Anticancer Drugs Based on Hypoxia Activatable Phototrigger Conjugated Chitosan Nanoparticles. *Adv. Mater.* **2013**, *25*, 1981−1986.

Table 2. Quantitative Analysis of Gene Expression Shown in Figure 8[a]

	CS				TPG/CS			
osteoblast-related genes	day 1	day 2	day 4	day 7	day 1	day 2	day 4	day 7
Runx2	0.03 ± 0.0015	0.04 ± 0.0130	0.16 ± 0.0458	0.25 ± 0.0666	0.32 ± 0.0872	0.51 ± 0.0458	0.95 ± 0.0700	1.00 ± 0.0557
ALP	0.11 ± 0.0262	0.30 ± 0.0872	0.52 ± 0.0854	0.58 ± 0.0458	0.35 ± 0.0600	0.83 ± 0.0611	0.98 ± 0.0874	1.00 ± 0.0702
BMP-2	088 ± 0.0603	1.00 ± 0.0624	0.94 ± 0.1058	0.92 ± 0.0361	0.91 ± 0.0917	0.90 ± 0.0265	0.93 ± 0.0603	0.89 ± 0.0819
BMP-4	0.91 ± 0.0608	0.92 ± 0.1153	1 ± 0.0764	0.95 ± 0.0300	0.89 ± 0.0800	0.91 ± 0.0458	0.92 ± 0.0794	0.93 ± 0.0529

[a]Expression of the markers was normalized to the expression of the housekeeping gene GAPDH. Values presented as mean ± standard deviation from triplicate measurements; for comparison, highest values were set to 1.00.

DOI: 10.1021/acsami.5b06300
ACS Appl. Mater. Interfaces 2015, 7, 20893−20901

(5) Zhang, W.; Li, X.; Zou, R. Multifunctional Glucose Biosensors From Fe_3O_4 Nanoparticles Modified Chitosan/Graphene Nanocomposites. *Sci. Rep.* **2015**, *5*, 11129.
(6) Song, J. M.; Shin, S. H.; Kim, Y. D. Comparative Study of Chitosan/Fibroin-Hydroxyapatite and Collagen Membranes for Guided Bone Regeneration in Rat Calvarial Defects: Micro-Computed Tomography Analysis. *Int. J. Oral Sci.* **2014**, *6*, 87−93.
(7) Hassan, S.; Suzuki, M.; Abd El-Moneim, A. Synthesis of MnO_2-chitosan Nanocomposite by One-Step Electrodeposition for Electrochemical Energy Storage Application. *J. Power Sources* **2014**, *246*, 68−73.
(8) Zhang, M.; Li, X. H.; Gong, Y. D. Properties and Biocompatibility of Chitosan Films Modified by Blending with PEG. *Biomaterials* **2002**, *23*, 2641−2648.
(9) Mazaheri, M.; Akhavan, O.; Simchi, A. Flexible Bactericidal Graphene Oxide-Chitosan Layers for Stem Cell Proliferation. *Appl. Surf. Sci.* **2014**, *301*, 456−462.
(10) Pok, S.; Vitale, F.; Eichmann, S. L. Biocompatible Carbon Nanotube-Chitosan Scaffold Matching the Electrical Conductivity of the Heart. *ACS Nano* **2014**, *8*, 9822−9832.
(11) Bao, H.; Pan, Y.; Ping, Y. Chitosan-Functionalized Graphene Oxide as a Nanocarrier for Drug and Gene Delivery. *Small* **2011**, *7*, 1569−1578.
(12) Hu, S.; Zeng, Y.; Yang, S. Application of Graphene Based Nanotechnology in Stem Cells Research. *J. Nanosci. Nanotechnol.* **2015**, *15*, 6327−6341.
(13) Weng, Z.; Xu, Z.; Gao, C. Highly Oxidized Graphene with Enhanced Fluorescence and its Direct Fluorescence Visualization. *Sci. China: Chem.* **2014**, *57*, 605−614.
(14) Geim, A. K.; Novoselov, K. S. The Rise of Graphene. *Nat. Mater.* **2007**, *6*, 183−191.
(15) Pak, S. W.; Cho, S. G.; Lee, D. U. Thermal Annealing Effects On ZnO Films Grown On Graphene Buffered Si Substrates. *J. Nanosci. Nanotechnol.* **2014**, *14*, 8804−8807.
(16) Zhang, L.; Wang, Z.; Lu, Z. PEGylated Reduced Graphene Oxide as a Superior ssRNA Delivery System. *J. Mater. Chem. B* **2013**, *1*, 749−755.
(17) Shao, D.; Li, J.; Wang, X. Poly(Amidoxime)-Reduced Graphene Oxide Composites as Adsorbents for the Enrichment of Uranium From Seawater. *Sci. China: Chem.* **2014**, *57*, 1449−1458.
(18) Zhang, L.; Lu, Z.; Bai, Y. PEGylated Denatured Bovine Serum Albumin Modified Water-Soluble Inorganic Nanocrystals as Multifunctional Drug Delivery Platforms. *J. Mater. Chem. B* **2013**, *1*, 1289−1295.
(19) Kim, J.; Lee, M.; Jeon, S. Highly Transparent and Stretchable Field-Effect Transistor Sensors Using Graphene-Nanowire Hybrid Nanostructures. *Adv. Mater.* **2015**, *27*, 3292−3297.
(20) Vlassiouk, I.; Polizos, G.; Cooper, R. Strong and Electrically Conductive Graphene-Based Composite Fibers and Laminates. *ACS Appl. Mater. Interfaces* **2015**, *7*, 10702−10709.
(21) Novoselov, K. S.; Geim, A. K.; Morozov, S. V. Electric Field Effect in Atomically Thin Carbon Films. *Science* **2004**, *306*, 666−669.
(22) Cai, W.; Piner, R. D.; Stadermann, F. J. Synthesis and Solid-State NMR Structural Characterization of (13)C-labeled Graphite Oxide. *Science* **2008**, *321*, 1815−1817.
(23) Si, Y.; Samulski, E. T. Synthesis of Water Soluble Graphene. *Nano Lett.* **2008**, *8*, 1679−1682.
(24) Hashemi, E.; Akhavan, O.; Shamsara, M. Cyto and Genotoxicities of Graphene Oxide and Reduced Graphene Oxide Sheets On Spermatozoa. *RSC Adv.* **2014**, *4*, 27213−27223.
(25) Wang, Y.; Shi, Z.; Yin, J. Facile Synthesis of Soluble Graphene via a Green Reduction of Graphene Oxide in Tea Solution and its Biocomposites. *ACS Appl. Mater. Interfaces* **2011**, *3*, 1127−1133.
(26) Akhavan, O. KMAZ. Increasing the Antioxidant Activity of Green Tea Polyphenols Increasing the Antioxidant Activity of Green Tea Polyphenols in the Presence of Iron for the Reduction of Graphene Oxide. *Carbon* **2012**, *50*, 3015−3025.
(27) Thangapazham, R. L.; Singh, A. K.; Sharma, A. Green Tea Polyphenols and its Constituent Epigallocatechin Gallate Inhibits Proliferation of Human Breast Cancer Cells in Vitro and in Vivo. *Cancer Lett.* **2007**, *245*, 232−241.
(28) Ghosh, D.; Scheepens, A. Vascular Action of Polyphenols. *Mol. Nutr. Food Res.* **2009**, *53*, 322−331.
(29) Hoshikawa, S.; Nakagawa, Y.; Ozaki, H. Effects of Green Tea Polyphenols OnIodide-Induced Autoimmune Thyroiditis in Nonobese Diabetic Mice. *Immunol. Invest.* **2013**, *42*, 235−246.
(30) Shen, C.; Chyu, M.; Wang, J. Tea and Bone Health: Steps Forward in Translational Nutrition. *Am. J. Clin. Nutr.* **2013**, *98*, 1694S−1699S.
(31) Shen, C.; Yeh, J. K.; Stoecker, B. J. Green Tea Polyphenols Mitigate Deterioration of Bone Microarchitecture in Middle-Aged Female Rats. *Bone* **2009**, *44*, 684−690.
(32) Abdolahad, M.; Janmaleki, M.; Mohajerzadeh, S. Polyphenols Attached Graphene Nanosheets for High Efficiency NIR Mediated Photodestruction of Cancer Cells. *Mater. Sci. Eng., C* **2013**, *33*, 1498−1505.
(33) Calizo, I.; Balandin, A. A.; Bao, W. Temperature Dependence of the Raman Spectra of Graphene and Graphene Multilayers. *Nano Lett.* **2007**, *7*, 2645−2649.
(34) Akhavan, O. Bacteriorhodopsin as a Superior Substitute for Hydrazine in Chemical Reduction of Single-Layer Graphene Oxide Sheets. *Carbon* **2015**, *81*, 158−166.
(35) Gadgil, B.; Damlin, P.; Heinonen, M. A Facile One Step Electrostatically Driven Electrocodeposition of Polyviologen-Reduced Graphene Oxide Nanocomposite Films for Enhanced Electrochromic Performance. *Carbon* **2015**, *89*, 53−62.
(36) Justin, R.; Chen, B. Characterisation and Drug Release Performance of Biodegradable Chitosan-Graphene Oxide Nanocomposites. *Carbohydr. Polym.* **2014**, *103*, 70−80.
(37) Wang, G.; Xu, X.; Qiu, L. Dual Responsive Enzyme Mimicking Activity of AgX (X = Cl, Br, I) Nanoparticles and its Application for Cancer Cell Detection. *ACS Appl. Mater. Interfaces* **2014**, *6*, 6434−6442.
(38) El Achaby, M.; Essamlali, Y.; El Miri, N. Graphene Oxide Reinforced Chitosan/Polyvinylpyrrolidone Polymer Bio-Nanocomposites. *J. Appl. Polym. Sci.* **2014**, *131*, 41042.
(39) Li, M.; Wang, Y.; Liu, Q. In Situ Synthesis and Biocompatibility of Nano Hydroxyapatite On Pristine and Chitosan Functionalized Graphene Oxide. *J. Mater. Chem. B* **2013**, *1*, 475−484.
(40) Jiang, W.; Lai, K.; Liu, K. "Green" Functionalization of Magnetic Nanoparticles Via Tea Polyphenol for Magnetic Resonance/Fluorescent Dual-Imaging. *Nanoscale* **2014**, *6*, 1305−1310.
(41) Shibukawa, M.; Kondo, Y.; Ogiyama, Y. Interfacial Water On Hydrophobic Surfaces Recognized by Ions and Molecules. *Phys. Chem. Chem. Phys.* **2011**, *13*, 15925−15935.
(42) Cui, W.; Li, X.; Xie, C. Hydroxyapatite Nucleation and Growth Mechanism On Electrospun Fibers Functionalized with Different Chemical Groups and their Combinations. *Biomaterials* **2010**, *31*, 4620−4629.
(43) Wang, P.; Zhao, L.; Liu, J. Bone Tissue Engineering via Nanostructured Calcium Phosphate Biomaterials and Stem Cells. *Bone Res.* **2014**, *2*, 14017.
(44) Rahman, M. S.; Akhtar, N.; Jamil, H. M. TGF-beta/BMP Signaling and Other Molecular Events: Regulation of Osteoblastogenesis and Bone Formation. *Bone Res.* **2015**, *3*, 15005.
(45) Grottkau, B. E.; Yang, X.; Zhang, L. Comparison of Effects of Mechanical Stretching on Osteogenic Potential of ASCs and BMSCs. *Bone Res.* **2013**, *1*, 282−290.
(46) He, G.; Guo, B.; Wang, H. Surface Characterization and Osteoblast Response to a Functionally Graded Hydroxyapatite/Fluoro-Hydroxyapatite/Titanium Oxide Coating On Titanium Surface by Sol-Gel Method. *Cell Proliferation* **2014**, *47*, 258−266.
(47) Siddiqui, S.; Ahmad, E.; Gupta, M. Cissus Quadrangularis Linn Exerts Dose-Dependent Biphasic Effects: Osteogenic and Anti-Proliferative, through Modulating ROS, Cell Cycle and Runx2 Gene Expression in Primary Rat Osteoblasts. *Cell Proliferation* **2015**, *48*, 443−454.

DOI: 10.1021/acsami.5b06300
ACS Appl. Mater. Interfaces 2015, 7, 20893−20901

(48) Alzhavan, O.; Ghaderi, E.; Shahsavar, M. Graphene Nanogrids for Selective and Fast Osteogenic Differentiation of Human Mesenchymal Stem Cells. *Carbon* **2013**, *59*, 200−211.
(49) Engler, A. J.; Sen, S.; Sweeney, H. L.; Discher, D. E. Matrix Elasticity Directs Stem Cell Lineage Specification. *Cell* **2006**, *126*, 677−689.

DOI: 10.1021/acsami.5b06300
ACS Appl. Mater. Interfaces 2015, 7, 20893−20901